An inversion formula for the cone-beam transform for arbitrary source trajectories

Birsen Yazıcı, *Senior Member IEEE*, Zhengmin Li and Jed Pack

***Abstract*—We introduce a forward model for the cone-beam X-ray Computed Tomography projection data measured in native geometries as a Fourier Integral Operator and present a corresponding filtered-backprojection type inversion formula. Our model and inversion formula can accommodate arbitrary source trajectories, arbitrary detector plane orientation, detector surface geometries, and other system related parameters. When the model parameters are chosen such that the forward model is equivalent to the cone-beam transform with helical or circular source trajectory, the inversion formula leads to the well-known Feldkamp's method with the one-dimensional filtering in the tangential direction. In the final version of the manuscript we will present validation of the inversion formula using the cone-beam projection data generated using GE's software package CatSim.**

I. Introduction

In practice, most of the existing cone-beam reconstruction methods are designed for the circular and helical source trajectories. They utilize a standard data acquisition geometry, in which the detector plane is perpendicular to the central ray, and parallel to the axial-axis. However, reconstruction methods for more general source trajectories and detector plane orientations are desirable in various applications [1] [2] [3]. In this paper, we introduce a new analytic forward model for the cone-beam projection data obtained in its native geometries in the form of a Fourier Integral Operator (FIO). The model reduces to the standard cone-beam transform when the amplitude term of the FIO is set to a certain function. We, next, introduce a filtered-backprojection (FBP) type inversion method for the new forward model. The model and the associated inversion method can accommodate arbitrary source trajectories, detector surface geometry and orientation, and other system related parameters, such as the physical detector size and the focal spot size. When the source trajectory is restricted to a helix and when the detector surface is planar with the cone axis perpendicular to the detector plane, our inversion formula reduces to the Feldkamp's (FDK) formula for the helical trajectory with one-dimensional tangential filtering.

Our approach has several advantages as compared to the idealized X-ray transform and associated inversion methods: 1) The new forward model can provide a more realistic representation of the cone-beam CT projection data than the idealized X-ray transform. As a result, our inversion method can provide a better reconstruction method than that of approximate or exact X-ray transform inversion methods. 2) Our model and inversion method can accommodate arbitrary imaging geometries including source trajectory, detector surface geometries and orientations. 3) Our model and inversion formula are both analytic and can be implemented computationally efficiently with the computational complexity of fast-backprojection algorithms [4]. 4) The measurement noise and a priori object statistics can be incorporated into our model and reconstruction formula [5]. 5) The point spread function of our reconstruction formula can be studied by microlocal analysis.

The paper is organized as follows: In Section II, we introduce the cone-beam transform for arbitrary source trajectories and briefly describe the general FIO-based model for cone-beam projection data. In Section III, we present our FBP-type inversion formula. In Section IV, we show the equivalence of our inversion formula with the FDK's method for the circular source trajectory and comment on the relationship of our method to other methods. Section IV concludes our discussion. In the final version of the manuscript, we will present simulation results using the X-ray CT simulation package CatSim developed by GE.

II. Cone-beam Transform as a Fourier Integral Operator In Its Native Geometry

We consider the imaging geometry shown in Fig.1. We

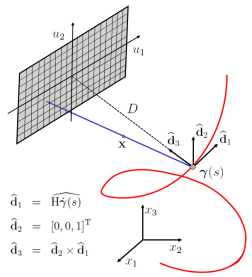

Fig. 1: Local coordinate system for the cone-beam projection measurements for a planar detector geometry. Vectors $\widehat{\mathbf{d}}_1$ and $\widehat{\mathbf{d}}_2$ are parallel to the u_1 and u_2 axis of the detector plane, and the vector $\widehat{\mathbf{d}}_3$ is orthogonal to the detector plane. $\widehat{\mathbf{d}}_3$ is the unit vector pointing from the source location $\boldsymbol{\gamma}(s)$ to the point whose location is $(0,0)$ on the detector plane.

assume a coordinate system where the x_-axis is perpendicular to the axial plane spanned by the unit vectors along x_1- and x_2-axes shown in Fig.1. We assume that the detector plane is perpendicular to the axial plane. Furthermore, we assume that the horizontal axis of the detector plane remains parallel to the tangent vector of the source trajectory; and the cone axis

is perpendicular to the detector plane. These assumptions are all consistent with the practical X-ray CT systems.

Let $\boldsymbol{\gamma}(s) \in \mathbb{R}^3$, $s \in [s_0,\ s_1]$, be a smooth trajectory for the X-ray source, and S^2 be the unit sphere in $\mathbb{R}^3$. Let $\hat{\mathbf{r}} \in S^2$ be the unit vector originating from the source position $\boldsymbol{\gamma}(s)$. We define the local coordinate system shown in Fig.1 as follows:

$$\begin{aligned} \widehat{\mathbf{d}}_1 &= \widehat{\mathrm{H}\dot{\boldsymbol{\gamma}}(s)} \\ \widehat{\mathbf{d}}_2 &= [0,0,1]^{\mathrm{T}} \\ \widehat{\mathbf{d}}_3 &= \widehat{\mathbf{d}}_2 \times \widehat{\mathbf{d}}_1 \end{aligned} \tag{1}$$

where $\mathrm{H} = \begin{bmatrix} 1 & 0 & 0 \\ 0 & 1 & 0 \\ 0 & 0 & 0 \end{bmatrix}$.

We assume that the detector array consists of $N_r \times N_c$ detector units. We use the pair $[u_1, u_2]$ to indicate the detector position, which are signed distances along $\widehat{\mathbf{d}}_1$ and $\widehat{\mathbf{d}}_2$. We assume that the axis of the cone when the source is at $\boldsymbol{\gamma}(s)$ intersects the detector plane at the $[u_1, u_2] = (0,0)$ of the detector plane. Let D be the distance between the source and the detector plane. Given the source location and the distance D, $[u_1, u_2]$ can be determined by the rotation angle s.

The line equation of the X-ray, which goes through $\mathbf{x}$ and projects onto $[u_1, u_2]$ in the detector plane, can be defined as the intersection of the following two planes:

$$u_1 = D\frac{(\mathbf{x}-\boldsymbol{\gamma}(s))\cdot\widehat{\mathbf{d}}_1}{(\mathbf{x}-\boldsymbol{\gamma}(s))\cdot\widehat{\mathbf{d}}_3} \tag{2}$$

$$u_2 = D\frac{(\mathbf{x}-\boldsymbol{\gamma}(s))\cdot\widehat{\mathbf{d}}_2}{(\mathbf{x}-\boldsymbol{\gamma}(s))\cdot\widehat{\mathbf{d}}_3}. \tag{3}$$

Thus, we write the cone-beam transform as follows:

$$\begin{aligned} d(u_1,u_2,s) = \int &\delta\Big(u_1 - D\frac{(\mathbf{x}-\boldsymbol{\gamma}(s))\cdot\widehat{\mathbf{d}}_1}{(\mathbf{x}-\boldsymbol{\gamma}(s))\cdot\widehat{\mathbf{d}}_3}\Big) \\ &\delta\Big(u_2 - D\frac{(\mathbf{x}-\boldsymbol{\gamma}(s))\cdot\widehat{\mathbf{d}}_2}{(\mathbf{x}-\boldsymbol{\gamma}(s))\cdot\widehat{\mathbf{d}}_3}\Big) \\ &\times\frac{D^2|\mathbf{x}-\boldsymbol{\gamma}(s)|}{((\mathbf{x}-\boldsymbol{\gamma}(s))\cdot\widehat{\mathbf{d}}_1)^3} f(\mathbf{x})\mathrm{d}\mathbf{x}. \end{aligned} \tag{4}$$

To simplify our notation we define

$$\begin{aligned} \rho_1(\mathbf{x},s) &:= D\frac{(\mathbf{x}-\boldsymbol{\gamma}(s))\cdot\widehat{\mathbf{d}}_1}{(\mathbf{x}-\boldsymbol{\gamma}(s))\cdot\widehat{\mathbf{d}}_3} \\ \rho_2(\mathbf{x},s) &:= D\frac{(\mathbf{x}-\boldsymbol{\gamma}(s))\cdot\widehat{\mathbf{d}}_2}{(\mathbf{x}-\boldsymbol{\gamma}(s))\cdot\widehat{\mathbf{d}}_3} \\ \boldsymbol{\rho}(\mathbf{x},s) &:= [\rho_1(\mathbf{x},s),\ \rho_2(\mathbf{x},s)] \end{aligned}$$

and

$$\begin{aligned} \boldsymbol{u} &:= [u_1,\ u_2] \\ A(\mathbf{x},s) &:= \frac{D^2|\mathbf{x}-\boldsymbol{\gamma}(s)|}{((\mathbf{x}-\boldsymbol{\gamma}(s))\cdot\widehat{\mathbf{d}}_1)^3}. \end{aligned}$$

We rewrite Eq. (4) as follows:

$$d(\boldsymbol{u},s) = \int \delta(\boldsymbol{u}-\boldsymbol{\rho}(\mathbf{x},s))A(\mathbf{x},s)f(\mathbf{x})\mathrm{d}\mathbf{x}. \tag{5}$$

Alternatively, we can express (5) as:

$$\begin{aligned} d(\boldsymbol{u},s) &= \mathcal{F}[f](\mathbf{u},s) \\ &:= \frac{1}{4\pi^2}\int \mathrm{e}^{\mathrm{i}\boldsymbol{\omega}\cdot(\boldsymbol{u}-\boldsymbol{\rho}(\mathbf{x},s))}A(\mathbf{x},s)f(\mathbf{x})\mathrm{d}\boldsymbol{\omega}\mathrm{d}\mathbf{x}. \end{aligned} \tag{6}$$

Eq. (6) shows that the cone-beam transform $\mathcal{F}$ is an FIO [6] with its phase term equal to

$$\phi(\boldsymbol{\omega},\mathbf{x},\boldsymbol{u},s) = \boldsymbol{\omega}\cdot(\boldsymbol{u}-\boldsymbol{\rho}(\mathbf{x},s)) \tag{7}$$

and its amplitude term equal to

$$A(\mathbf{x},s) = \frac{D^2|\mathbf{x}-\boldsymbol{\gamma}(s)|}{((\mathbf{x}-\boldsymbol{\gamma}(s))\cdot\widehat{\mathbf{d}}_1)^3}.$$

Since the critical points of the model in (7) are given by the line passing through the source and the point $[u_1, u_2]$ on the detector plane, we define the general forward model for the cone-beam projection data by the following model:

$$\begin{aligned} d(\boldsymbol{u},s) &= \mathcal{F}[f](\mathbf{u},s) \\ &= \frac{1}{4\pi^2}\int \mathrm{e}^{\mathrm{i}\boldsymbol{\omega}\cdot(\boldsymbol{u}-\boldsymbol{\rho}(\mathbf{x},s))}A(\boldsymbol{\omega},\mathbf{x},\boldsymbol{u},s)f(\mathbf{x})\mathrm{d}\boldsymbol{\omega}\mathrm{d}\mathbf{x} \end{aligned} \tag{8}$$

where the amplitude factor A is a slowly decaying function that depends on the underlying system parameters and geometric correction factors. Note that the amplitude factor in (8) depends not only on $\mathbf{x}$ and s, but also on $\boldsymbol{\omega}$ and $\boldsymbol{u}$.

III. A FBP-type inversion of the cone-beam transform

We form an image by means of a filtered-backprojection operator as follows:

$$\begin{aligned} I(\mathbf{z}) &= \mathcal{K}[d](\mathbf{z}) \\ &= \int \mathrm{e}^{-\mathrm{i}\phi(\boldsymbol{\omega},\mathbf{z},\boldsymbol{u},s)}Q(\boldsymbol{\omega},\mathbf{z},s)d(\boldsymbol{u},s)\mathrm{d}\boldsymbol{\omega}\mathrm{d}\boldsymbol{u}\mathrm{d}s \end{aligned} \tag{9}$$

where $I(\mathbf{z})$ is the reconstructed image, $\mathcal{K}$ is the filtered-backprojection operator, and Q is the filter to be determined below.

Substituting (6) into (9), we obtain

$$I(\mathbf{z}) = \mathcal{K}\mathcal{F}[f](\mathbf{z}) = \int L(\mathbf{z},\mathbf{x})f(\mathbf{x})\mathrm{d}\mathbf{x} \tag{10}$$

where

$$\begin{aligned} L(\mathbf{z},\mathbf{x}) = \int &\mathrm{e}^{\mathrm{i}\left(\phi(\boldsymbol{\omega},\mathbf{x},\boldsymbol{u},s)-\phi(\boldsymbol{\omega}',\mathbf{z},\boldsymbol{u},s)\right)}A(\mathbf{x},s) \\ &Q(\boldsymbol{\omega}',\mathbf{z},s)\mathrm{d}\boldsymbol{\omega}\mathrm{d}\boldsymbol{\omega}'\mathrm{d}\boldsymbol{u}\mathrm{d}s. \end{aligned} \tag{11}$$

Applying the method of stationary phase and evaluating the $\mathrm{d}\boldsymbol{u}$ integration above, we obtain

$$L(\mathbf{z},\mathbf{x}) = \int \mathrm{e}^{\mathrm{i}\boldsymbol{\omega}\cdot(\boldsymbol{\rho}(\mathbf{x},s)-\boldsymbol{\rho}(\mathbf{z},s))}A(\mathbf{x},s)Q(\boldsymbol{\omega},\mathbf{z},s)\mathrm{d}\boldsymbol{\omega}\mathrm{d}s. \tag{12}$$

The kernel L of $\mathcal{K}\mathcal{F}$ is the point spread function (PSF) of the imaging operator $\mathcal{K}$. $L(\mathbf{z},\mathbf{x})$ represents the reconstructed image at pixel $\mathbf{z}$ due to a point object located at $\mathbf{x}$.

Let

$$\varphi(\mathbf{z},\mathbf{x},\boldsymbol{\omega},s) = \boldsymbol{\omega}\cdot\left(\boldsymbol{\rho}(\mathbf{x},s)-\boldsymbol{\rho}(\mathbf{z},s)\right). \tag{13}$$

The main contributions to $L(\mathbf{z},\mathbf{x})$ come from the critical points of the phase of $\mathcal{KF}$, satisfying the following conditions:

$$\frac{\partial\varphi}{\partial\boldsymbol{\omega}} = 0 \quad \Rightarrow \quad \boldsymbol{\rho}(\mathbf{x},s)=\boldsymbol{\rho}(\mathbf{z},s) \tag{14}$$

$$\frac{\partial\varphi}{\partial s} = 0 \quad \Rightarrow \quad \partial_s\boldsymbol{\rho}(\mathbf{x},s)=\partial_s\boldsymbol{\rho}(\mathbf{z},s). \tag{15}$$

Thus, we recover the singularities of the object at the intersection of the locus points of the two three-dimensional manifolds defined above.

Assuming that the only contribution to the pixel at $\mathbf{z}$ comes from $\mathbf{x}$, we approximate φ as follows:

$$\begin{aligned}\varphi(\mathbf{z},\mathbf{x},\boldsymbol{\omega},s) &\approx (\mathbf{z}-\mathbf{x})\cdot\nabla\varphi(\mathbf{z},\mathbf{x},\boldsymbol{\omega},s)\\ &= (\mathbf{z}-\mathbf{x})\cdot\nabla\boldsymbol{\omega}\cdot\boldsymbol{\rho}(\mathbf{z},s)|_{\mathbf{z}=\mathbf{x}}.\end{aligned} \tag{16}$$

Let

$$\boldsymbol{\xi} = \nabla\boldsymbol{\omega}\cdot\boldsymbol{\rho}(\mathbf{z},s)|_{\mathbf{z}=\mathbf{x}}. \tag{17}$$

We now make the following change of variables:

$$(\boldsymbol{\omega},s)\rightarrow\boldsymbol{\xi}$$

and obtain

$$\begin{aligned}I(\mathbf{z}) \approx \int_{\Omega_{\mathbf{z}}} \mathrm{e}^{\mathrm{i}(\mathbf{z}-\mathbf{x})\cdot\boldsymbol{\xi}} \mid \frac{\partial(\boldsymbol{\omega},s)}{\partial\boldsymbol{\xi}} \mid A(\mathbf{z},s(\boldsymbol{\xi}))\\ Q(\boldsymbol{\omega}(\boldsymbol{\xi}),\mathbf{z},s(\boldsymbol{\xi}))f(\mathbf{x})\mathrm{d}\boldsymbol{\xi}\mathrm{d}\mathbf{x}\end{aligned} \tag{18}$$

where $|\frac{\partial(\boldsymbol{\omega},s)}{\partial\boldsymbol{\xi}}|$ is the determinant of the Jacobian that comes from the change of variables in (17), and $s(\boldsymbol{\xi})$ and $\boldsymbol{\omega}(\boldsymbol{\xi})$ represent s and $\boldsymbol{\omega}$ in terms of $\boldsymbol{\xi}$; and $\Omega_{\mathbf{z}}$ is the data collection manifold defined as

$$\Omega_{\mathbf{z}} = \{\boldsymbol{\xi}=\nabla\boldsymbol{\omega}\cdot\boldsymbol{\rho}(\mathbf{x},s)|_{\mathbf{x}=\mathbf{z}} \mid |\frac{\partial(\boldsymbol{\omega},s)}{\partial\boldsymbol{\xi}}|\neq 0 \;\&\; A(\boldsymbol{\omega},\mathbf{z})\neq 0\}. \tag{19}$$

We determine the filter Q so that the kernel L of the PSF is approximately a Dirac-delta function, i.e.,

$$L(\mathbf{x},\mathbf{z})\approx\delta(\mathbf{x}-\mathbf{z}).$$

We set

$$Q(\boldsymbol{\xi},\mathbf{z}) = \frac{\chi_\Omega}{A(s(\boldsymbol{\xi}),\mathbf{z})}|\frac{\partial\boldsymbol{\xi}}{\partial(\boldsymbol{\omega},s)}|, \quad \boldsymbol{\xi}\in\Omega_{\mathbf{z}} \tag{20}$$

where $\chi_{\Omega_{\mathbf{z}}}$ is a smooth cut-off function that prevents division by zero.

With this choice of filtering, the inverse map $\mathcal{K}$ reconstructs the visible singularities of the object not only at the right location and orientation, but also at the right strength.

The $\boldsymbol{\xi}$ vector is given as follows:

$$\begin{aligned}\boldsymbol{\xi} &= \nabla\boldsymbol{\omega}\cdot\boldsymbol{\rho}(\mathbf{x},s)|_{\mathbf{x}=\mathbf{z}}\\ &= \frac{D}{C_3^2(\mathbf{x},s)}\boldsymbol{\omega}\cdot\begin{bmatrix}\widehat{\mathbf{d}}_1C_3(\mathbf{x},s)-\widehat{\mathbf{d}}_3C_1(\mathbf{x},s)\\ \widehat{\mathbf{d}}_2C_3(\mathbf{x},s)-\widehat{\mathbf{d}}_3C_2(\mathbf{x},s)\end{bmatrix}\\ &= D\{\frac{\omega_1}{C_3(\mathbf{x},s)}\widehat{\mathbf{d}}_1+\frac{\omega_2}{C_3(\mathbf{x},s)}\widehat{\mathbf{d}}_2\\ &\quad -[\frac{\omega_1C_1(\mathbf{x},s)+\omega_2C_2(\mathbf{x},s)}{C_3^2(\mathbf{x},s)}]\widehat{\mathbf{d}}_3\}\end{aligned} \tag{21}$$

where $C_i(\mathbf{x},s)=(\mathbf{x}-\boldsymbol{\gamma}(s))\cdot\widehat{\mathbf{d}}_i,\ i=1,2,3$. Note that $C_3(\mathbf{x},s)=0$ corresponds to the case when the cone angle is 90 degrees, which is an unrealistic setting for all practical purposes. The vector $\boldsymbol{\xi}$ can be viewed as the Fourier component that contributes to the reconstruction of the pixel at $\mathbf{z}$ when the source is at $\boldsymbol{\gamma}(s)$. The vector $\boldsymbol{\xi}$ and the data collection manifold $\Omega_{\mathbf{z}}$ determine the resolution as well as many of the properties of the reconstructed image. Fig. 2 illustrates the $\boldsymbol{\xi}$ vector.

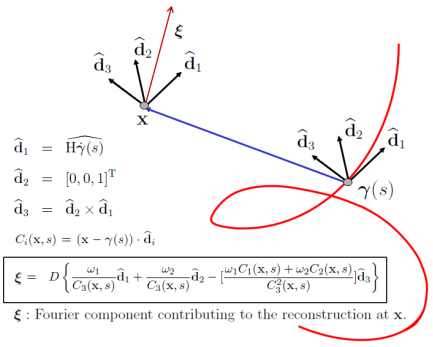

Fig. 2: The vector $\boldsymbol{\xi}$ represents the Fourier component contributing to the reconstruction of the object at $\mathbf{x}$.

IV. Inversion formula for the circular source trajectory

In this section, we discuss the equivalence of our inversion method to the existing approximate methods [7] for the circular source trajectory.

For the circular trajectory, $\boldsymbol{\gamma}(s)$ is given as follows:

$$\boldsymbol{\gamma}(s)=[R\cos(s),\ R\sin(s),\ 0],\ s\in\mathbb{R}^3, \tag{22}$$

where R denotes the radius of the circle. Substituting Eq. (22) and its derivative into Eq. (1), we obtain

$$\begin{bmatrix}\widehat{\mathbf{d}}_1\\ \widehat{\mathbf{d}}_2\\ \widehat{\mathbf{d}}_3\end{bmatrix}=\begin{bmatrix}-\sin(s) & \cos(s) & 0\\ 0 & 0 & 1\\ -\cos(s) & -\sin(s) & 0\end{bmatrix}.$$

Thus, for the circular trajectory, the filter in Eq. (20) becomes

$$Q(\boldsymbol{\omega},\mathbf{z},s)=\frac{DR}{C_3(\mathbf{z},s)|\mathbf{z}-\boldsymbol{\gamma}(s)|}|\omega_1|. \tag{23}$$

Substituting Q into Eq. (9), we obtain the FBP-type inversion formula for the circular source trajectory given as

$$\begin{aligned}I(\mathbf{z}) = \int \mathrm{e}^{\mathrm{i}(\omega_1 D\frac{(\mathbf{z}-\boldsymbol{\gamma}(s))\cdot\widehat{\mathbf{d}}_1}{(\mathbf{z}-\boldsymbol{\gamma}(s))\cdot\widehat{\mathbf{d}}_3}+\omega_2 D\frac{(\mathbf{z}-\boldsymbol{\gamma}(s))\cdot\widehat{\mathbf{d}}_2}{(\mathbf{z}-\boldsymbol{\gamma}(s))\cdot\widehat{\mathbf{d}}_3})}\\ \frac{DR}{C_3^2(\mathbf{z},s)|\mathbf{z}-\boldsymbol{\gamma}(s)|}|\omega_1|\hat{d}_{12}(\omega_1,\omega_2,s)ds d\omega_1\end{aligned}$$

where

$$\hat{d}_{12}(\omega_1,\omega_2,s)=\int d(u_1,u_2,s)\mathrm{e}^{-\mathrm{i}(\omega_1u_1+\omega_2u_2)}du_1du_2 \tag{24}$$

is the Fourier transform of $d(u_1,u_2,s)$ with respect to u_1,u_2 variables.

We rewrite the original FDK's formula using the local coordinate system introduced above and obtain:

$$I(\mathbf{z}) = \int \mathrm{e}^{\mathrm{i}(\omega_1 u_1+\omega_2 u_2)} \frac{RD^2}{\sqrt{D^2+u_1^2+u_2^2}[R+\mathbf{z}\cdot\widehat{\mathbf{d}}_3]^2} \hat{d}_{12}(\omega_1,\omega_2,s)|\omega_1|\mathrm{d}\omega_1\mathrm{d}\omega_2\mathrm{d}s \quad (25)$$

where u_1 and u_2 indicate the projection location on the planar detector plane of the reconstructed point $\mathbf{z}$, which are given as

$$u_1(\mathbf{z}) = \frac{D\mathbf{z}\cdot\widehat{\mathbf{d}}_1}{R+\mathbf{z}\cdot\widehat{\mathbf{d}}_3}$$

$$u_2(\mathbf{z}) = \frac{D\mathbf{z}\cdot\widehat{\mathbf{d}}_2}{R+\mathbf{z}\cdot\widehat{\mathbf{d}}_3}.$$

We now compare the weighting factor and the one-dimensional filter of the FDK's formula to the filter in our inversion formula. From the CT scanner geometry, we have

$$\frac{C_3(\mathbf{x},s)}{D} = \frac{|\mathbf{x}-\boldsymbol{\gamma}(s)|}{\sqrt{D^2+u_1^2+u_2^2}} \quad (26)$$

$$|\mathbf{x}-\boldsymbol{\gamma}(s)| = \frac{C_3(\mathbf{x},s)\sqrt{D^2+u_1^2+u_2^2}}{D} \quad (27)$$

$$C_3(\mathbf{x},s) = R+\mathbf{z}\cdot\widehat{\mathbf{d}}_3. \quad (28)$$

Inserting the above three relationships into our filter, we obtain the familiar weighting factor and the one-dimensional filter in the FDK's formula:

$$Q(\boldsymbol{\omega},\mathbf{z},s) = \frac{D}{C_3(\mathbf{x},s)|\mathbf{x}-\boldsymbol{\gamma}(s)|}|R\omega_1| = \frac{D^2R}{[R+\mathbf{z}\cdot\widehat{\mathbf{d}}_3]^2\sqrt{D^2+u_1^2+u_2^2}}|\omega_1|. \quad (29)$$

V. Simulation study of the inversion formula

To validate our analytic derivation, we performed the reconstruction of the FORBILD-like thorax phantom using our formula. The simulation results will be included in the final manuscript.The number of views per rotation: 984; the number of detector columns: 888; the detector size: 1 mm×1 mm; the thickness of each slice in z- direction: 0.625 mm; the distance from source to detector: 949 mm; and the distance from the origin to the detector plane: 545 mm.

The reconstructed image size is 512×512, and the pixel size in each slice is 0.25 mm×0.25 mm.

The reconstructed image is are shown in Fig. 3. The visual comparison and the comparison of the cross section of the reconstructed images show that t our inversion formula produce the acceptable images.

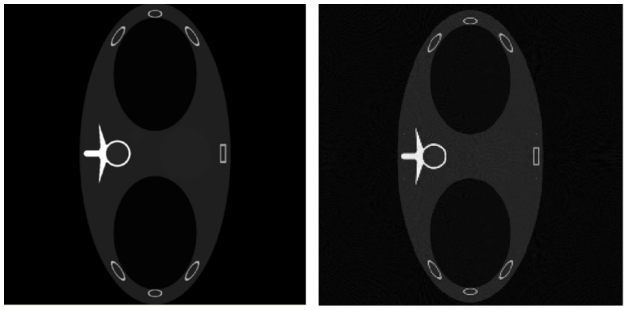

Fig. 3: Left: original center slice. Right :the reconstructed thorax phantom using our formula

VI. Conclusion

We present a new model for the cone-beam projection data in its native geometries and an FBP-type analytic reconstruction method for the model. Our model and inversion formula can accommodate arbitrary source trajectories, arbitrary detector orientation, detector surface geometry and other system related parameters. We showed the equivalency of our inversion formula to the FDK's formula for the circular trajectory both analytically and numerically.

In the final version of the manuscript we will present validation of the inversion formula using the cone-beam projection data generated using GE's software package CatSim.

References

[1] P. M. Shikhaliev, *Tilted angle CZT detector for photon counting/energy weighting x-ray and CT imaging,* Phys. Med. Biol., Vol.51, pp. 4267-4287, 2006

[2] J. D. Pack, F. Noo and H. Kudo, *Investigation of saddle trajectories for cardiac CT imaging in cone-beam geometry*, Phys. Med. Biol., Vol. 49, No. 11, pp. 2317-2336, 2004

[3] Z. Yu, *et al*, *Line plus arc source trajectories and their R-line coverage for long-object cone-beam imaging with a C-arm system,* Phys. Med. Biol., Vol.56 , pp. 3447-3471, 2011

[4] E. Candes, *et al*, *Fast computation of Fourier integral operators,* Applied and computational mathematics, Caltech, Pasadena, CA, 2006

[5] B. Yazici, M. Cheney and C.E. Yarman, *Synthetic aperture inversion in the presence of noise and clutter,* Inverse Problems, Vol. 22, pp. 1705-1729, 2006.

[6] F. Treves, *Introduction to Pseudodifferential and Fourier Integral Operators,* Vol. 1 and 2 Plemum Press, New York, 1980

[7] L.A. Feldkamp, L.C. Davis and J.W. Kress, *Practical cone-beam algorithm*, J.Opt.Soc. Am., Vol.1, No. 6, pp. 612-619, 1984

[8] G. Wang, *et al*, *A general cone-beam recosntruction algorithm,* IEEE Trans. on Med. Imag., Vol. 12, No. 3, pp. 486-495, 1993

[9] X. Yan and R. M Leahy, *Cone beam tomography with circular, elliptical and spiral orbits,* Phys. Med. Biol., Vol. 37, No. 3, pp. 493-506, 1992

[10] X. Yan and R. M Leahy, *Derivation and Analysis of a Filtered Backprojection Algorithm for Cone Beam Projection Data,*IEEE Trans. on Med. Imag., Vol.10. No. 3, pp. 462-412, 1991